Available online at www.sciencedirect.com

jmr&t Journal of Materials Research and Technology

journal homepage: www.elsevier.com/locate/jmrt

Enhanced UV blocking, tensile and thermal properties of bendable TEMPO-oxidized bacterial cellulose powder-based films immersed in PVA/*Uncaria gambir*/ZnO solution

Dieter Rahmadiawan [a,b], *Hairul Abral* [c,d,*], *Mohammad Khalid Ilham* [c], *Poppy Puspitasari* [e], *Rahmat Azis Nabawi* [b], *Shih-Chen Shi* [a], *Eni Sugiarti* [f], *Ahmad Novi Muslimin* [f], *Devi Chandra* [g], *R.A. Ilyas* [h], *Rahadian Zainul* [i]

[a] *Department of Mechanical Engineering, National Cheng Kung University (NCKU), Tainan, Taiwan*
[b] *Department of Mechanical Engineering, Universitas Negeri Padang, 25173 Padang, Sumatera Barat, Indonesia*
[c] *Laboratory of Nanoscience and Technology, Department of Mechanical Engineering, Andalas University, Padang 25163, Indonesia*
[d] *Research Collaboration Center for Nanocellulose, BRIN-Andalas University, Padang 25163, Indonesia*
[e] *Department of Mechanical Engineering, Faculty of Engineering, Universitas Negeri Malang, Semarang No. 5, Malang 65145, Indonesia*
[f] *Laboratory of High-Temperature Coating, Research Center for Physics Indonesian Institute of Sciences (LIPI) Serpong, Indonesia*
[g] *Department of Mechanical Engineering, Andalas University, Padang 25163, Indonesia*
[h] *School of Chemical and Energy Engineering, Faculty of Engineering, Universiti Teknologi Malaysia, Johor Bahru 81310, Malaysia*
[i] *Department of Chemistry, Faculty of Mathematics and Natural Science, Universitas Negeri Padang, West Sumatera 25171, Indonesia*

ARTICLE INFO

Article history:
Received 26 May 2023
Accepted 27 August 2023
Available online 29 August 2023

Keywords:
PVA
Bendable biocomposite
Environmentally friendly
TEMPO
Bacterial cellulose

ABSTRACT

The production of UV-resistant films from biomaterials is currently an active field of research. ZnO nanoparticle polymer fillers have been found to improve UV-light opacity. However, using ZnO as a filler is relatively expensive and time-consuming for film preparation. Substituting some of the ZnO nanoparticles with *Uncaria gambir* extract has been suggested to reduce the cost of film production, as the phenolic hydroxyl group present in *Uncaria gambir* provides excellent UV resistance. This study characterized dry bacterial cellulose (BC) powder-based films immersed without and with polyvinyl alcohol/*Uncaria gambir* extract/ZnO (M) solution for 2 and 5 min. It was found that BC/M biocomposites blocked 100% of the UV light while remaining transparent to visible wavelengths. These bendable biocomposite films also presented high tensile and thermal resistance properties. Immersion for 5 min increased significantly tensile strength, elongation at break, and toughness of the biocomposite to 77.2 MPa, 12.3%, and 5.8 MJ/m3, an increase of 130%, 748%, and 2409%, respectively, compared to uncoated BC film. These results suggest the

* Corresponding author. Laboratory of Nanoscience and Technology, Department of Mechanical Engineering, Andalas University, Padang 25163, Indonesia.
E-mail address: habral@yahoo.com (H. Abral).
https://doi.org/10.1016/j.jmrt.2023.08.267

immersion method could provide more efficient, environmentally friendly biocomposite films with significant UV resistance.

1. Introduction

Cellulose, a remarkable and abundant structural carbohydrate found in the cell walls of plants and certain algae, has long been a subject of scientific research [1]. Its unique properties, such as exceptional mechanical strength, biodegradability, and biocompatibility, have made it a valuable resource in various fields [2–5]. However, beyond the traditional plant-derived cellulose, an intriguing and biologically distinct form of this polymer has captured the attention of researchers and innovators - bacterial cellulose pellicle. Bacterial cellulose (BC) pellicle is a convenient, economical source of highly purified nanofibers. BC pellicle is comprises of long cellulose nanofibers interconnected to form a 3-D dimensional structure [6]. It can be used for various applications, including food packaging, lubricant additive, and sensor [7–11]. However, BC wet pellicle degrades quickly without supplementary treatment and requires a larger storage area than dried pellicle. Recently, a previous study successfully prepared dry microsized-BC powder from wet pellicle BC and used it as a base material for developing biocomposite films [12]. The biocomposites had good tensile and thermal properties, but their UV resistance has not yet been explored.

Exposure to ultraviolet (UV) radiation can cause the destruction of vitamins in food [13,14]. This harm can be prevented by minimizing direct contact with UV rays [15]. Several researchers have developed UV-absorbing biocomposite films through the incorporation of Zinc oxide (ZnO) nanoparticles [16–18]. In addition, UV light can also be blocked using lignin [19,20], melanin [21], and tannins [22,23]. As a phenolic compound, *Uncaria gambir* (UG) provides good protection from UV rays and also corrosion [24,25]. UG is environmentally friendly, cheap, and naturally available naturally in Siguntur, West Sumatra, Indonesia, where it is extracted from U. gambir Roxb. Leaves [26–29]. It is composed predominantly of catechin (a type of phenolic compound). Previous research has demonstrated that mixing UG with polyvinyl alcohol (PVA) improved the resulting biocomposite's UV shielding, which also had good transparency, tensile and thermal properties [24].

Pure PVA is a biodegradable polymer with excellent stretchability, water solubility, and biocompatibility [30–35]. This highly transparent, tough, and nontoxic synthetic material can form strong interactions with cellulose nanofibers through hydrogen bonding [36]. After the incorporation of the nanofibers, the tensile and thermal properties of PVA-based biocomposites improve further [37]. Unfortunately, even with nanofibres, PVA-based biocomposites with conventional preparation method has drawbacks. UG does not disperse as well through BC film as through PVA. ZnO, a nanoparticle with good transparency, has been proven to improve UV-light opacity [38–40]. However, using ZnO as a filler is relatively expensive and time-consuming for film preparation [41]. Substituting some of the ZnO nanoparticles with UG has been suggested to reduce the cost of film production because of the phenolic hydroxyl group present in UG. According to our previous study, UG alone provides superior UV resistance; hence, it is possible to replace the use of ZnO completely [24]. Therefore, this work investigates whether combining a BC film with PVA/UG/ZnO through the immersion method provides effective UV shielding.

Many studies have also focused on characterizing UV-resistant cellulose-based biocomposites prepared using various methods [16,22,42–44]. However, as far as we know, no previous studies have characterized the biocomposite film produced from dry BC powder-based film immersed in a solution of PVA/UG/ZnO nanoparticles (M). Immersion is a simple and efficient technique that improves the film's tensile and thermal properties [45]. Therefore, the present work provides valuable information about the characterization of pure BC film compared to BC/M biocomposites. We hypothesized that immersion of the transparent all-BC film into the suspension increases the strength, toughness, and thermal resistance of the BC/M biocomposite. It is hoped that adding both UG and ZnO should also provide almost complete shielding from the full range of UV wavelengths.

2. Materials and methods

2.1. Materials

Wet BC pellicle slabs (350 × 250 × 5 mm), were locally purchased from Padang, West Sumatera, Indonesia, and were previously utilized in our prior work [12]. The UG powder was obtained from the Sumatran Biota Laboratory, Andalas University, Padang. It was composed of catechins (91.8%), water (8.1%), and ash (0.1%). Sodium hydroxide (NaOH), sodium hypochlorite (NaClO), and sodium bromide (NaBr) were bought from PT. Brataco, Padang, Indonesia. 2,2,6,6-Tetramethylpiperidine-1-oxyl (TEMPO) was acquired from Sigma-Aldrich Co, USA. Pure PVA (MW: ~75,000 g/mol, >99% hydrolysis) and ZnO nanoparticles with particle size less than 100 nm were supplied by Sigma-Aldrich Pte. Ltd. Singapore.

2.2. Sample preparation

Wet BC pellicle slabs (length (35 cm), width (25 cm), and thickness (0.5 cm)) were soaked in 10% NaOH solution for 48 h. Then, distilled water was used to neutralize and clean the pellicle until pH 7. After that, it was crushed using a Maspion blender at 12000 rpm for 1 h. Next, the wet and refined pellicle was dried in a drying oven at 70 °C for 24 h. Then, the dried

pellicle was ground in an electric grinder at 3600 rpm for 1 h. The crushed BC powder was filtered through a 200-mesh filter.

The resulting BC powder (1 g) was oxidized using a solution of 200 g distilled water, 0.018 g TEMPO, 0.2 g NaBr, and 7.4 g NaClO at 50 °C. The mixture was stirred with a plate stirrer (Daihan Scientific MSH-200) at 350 rpm for 2 h. The suspension was cooled for 12 h and then neutralized until pH7 using distilled water. The pH7 suspension was homogenized at 8000 rpm for 30 min. Next, it was sonicated using a sonicator at 480 W for 20 min. The resulting BC suspension was cast in a Petri dish for drying at 50 °C for 24 h.

The UG (1 g) was mixed with distilled water (200 g). Then, it was heated at 70 °C and stirred with a hot plate stirrer (Daihan Scientific MSH-200) at 500 rpm for 30 min. 10 g PVA, and 0.1 g ZnO nanoparticles were added to the UG suspension. The mixture continued to be stirred for 4 h until it gelatinized. The dry BC film was immersed into the gelatinized PVA/UG/ZnO solution for 2 or 5 min. The non-immersed film and 2- and 5-min immersed films were labeled by NB0, NB2 and NB5, respectively.

2.3. Characterization

2.3.1. Film transparency

UV–Vis spectrophotometer (Shimadzu UV 1800, Japan) was operated to measure the transparency of the rectangular film (10 mm × 25 mm) in the range of 200–800 nm according to ASTM D 1003-00 [46].

2.3.2. Field emission scanning electron microscopy (FESEM)

FESEM (JEOL JFIB 4610, USA) with 10 kV, and 8 mA, was used to investigate the fracture surface morphology of the samples. The sample stub was used to anchor the sample. Minimization of static charge was achieved by coating the sample with carbon followed by gold for 30 s.

2.3.3. Tensile properties

A Com-Ten 95T series was used to investigate mechanical properties of the films, including tensile strength, tensile modulus, and elongation at the break according to the ASTM D638-Type V standard which is a standard test method for tensile properties of plastic materials [47]. Before testing, the samples were conditioned in a desiccator for 48 h at 50 ± 5% relative humidity and 25 °C. the thickness and width of the film were measured using a dial micrometer with 1 μm accuracy. The tests were repeated five times for each sample to acquire reliable results. Toughness of film was based on the area under the stress-strain curve [48]. Software from OriginPro 2016 was used to calculate it automatically.

2.3.4. Fourier transform infrared spectroscopy (FTIR)

FTIR spectra were recorded by PerkinElmer Frontier equipment (PerkinElmer, Inc., USA). First, the sample was dried using an oven at 50 °C until its weight was constant via checking periodically. Then, the dried sample was scanned at a frequency range of 4000–600 cm^{-1}.

2.3.5. X-Ray diffraction (XRD) testing

Samples were stored in a closed chamber with RH 50% for 24 h before XRD characterization. XRD testing was performed using PANalytical Xpert PRO (Philips Analytical, Netherlands) at 25 °C, 40 kV, and 30 mA. The samples were scanned from 2θ = 7.5° to 90°. The crystallinity index (CI) was measured using Eq. (1) [49]:

$$CI\ (\%) = \frac{(I_{max} - I_{am})}{I_{max}} \times 100 \quad (1)$$

where I_{max} is the peak intensity of a diffraction peak at about 2θ of 19.5° to 23°. I_{am} is the minimum intensity of the peak of the amorphous fraction.

2.3.6. Thermogravimetry analysis (TGA), and (DTG)

The thermal properties of the samples (TGA and DTG) were measured using a thermal analysis instrument DTG-60 from Shimadzu serial number C30565000570 (Kyoto, Japan) equipped with a TA-60WS thermal analyzer, FC-60A flow controller and TA-60 software. The sample was placed into the instrument set up with a nitrogen flow rate of 50 mL/min and a heating rate of 20 °C/min.

2.3.7. Statistical analysis

The significance of tensile properties for all samples was calculated using variance (ANOVA). Differences were examined using Duncan's multiple range test and were significant at $p \leq 0.05$.

3. Results and discussions

3.1. Physical film appearance

Fig. 1a–c present pure BC and biocomposite film photographs with various immersion times in the PVA/UG/ZnO matrix (M). The pure BC film is the most transparent. After immersing it in the M solution, however, the transparency decreased as shown in Fig. 1b and c. As expected, the lowest transparency was measured on the films immersed for 5 min. Despite this decreasing transparency, a university logo is still clearly visible under the BC/M film in Fig. 1b,c and e shows light transmission across the 200–800 nm wavelength range. BC film transmitted 70.3% light at 400 nm UV radiation. In contrast, the BC/M biocomposites absorb almost 100% of UV light at this wavelength. This result is probably due to the high UV light absorption of UG and ZnO [18,24]. The phenolic groups of UG contain unsaturation bonds and function as chromophores absorbing UV light [42,50]. This finding is similar to previous work reporting high UV shielding from a PVA-based film mixed with the polyphenol compounds from tannins [30].

3.2. Field emission scanning electron microscopy

Fig. 2 presents the FESEM morphology of the fractured surface of the tensile specimen. The morphological fracture surface of the M sample (Fig. 2a) exhibits highly pulled-out segments (yellow arrow), confirming significant plastic deformation. ZnO nanoparticles in PVA/UG matrix also show good dispersion, as no agglomeration or clustering is detected (red arrow). Fig. 2b shows the NB0 fracture surface with a sparse fiber configuration and non-compacted film structures, indicative

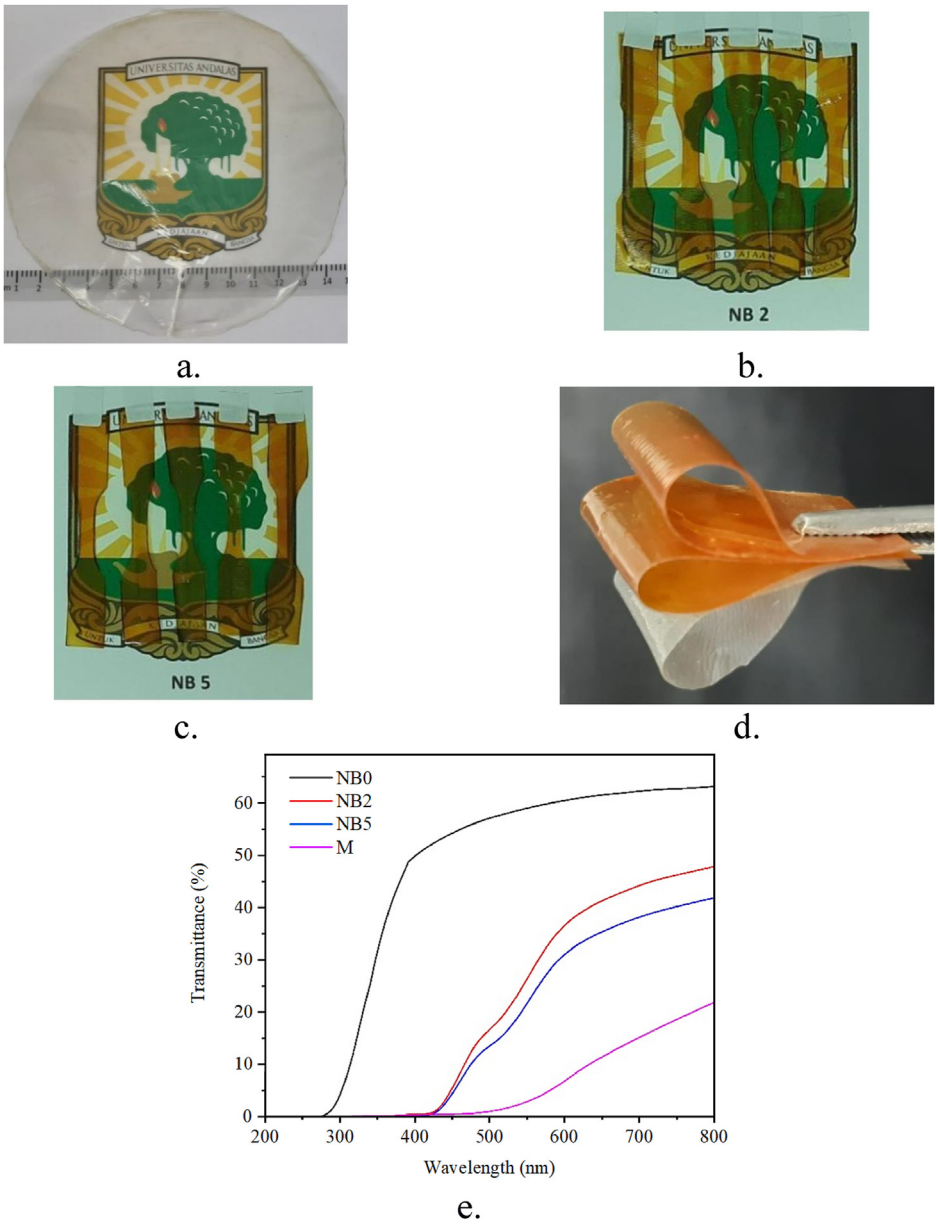

Fig. 1 – (a) a 21 μm thick and transparent NB0 film, (b) physical appearance for NB2, (c) NB5 films thicknesses of about 84 μm and 92 μm, respectively, (d) bendable biocomposite films without and with the matrix, and (e) transmittance values for each sample.

of defects resulting in a weak NB0 film. However, after immersion, the diffusivity of the PVA/UG/ZnO suspension into the NB0 film increased, filling the gaps between the fibers. Fig. 2c presents the fractured surface of the NB2 film, showing a relatively thin M layer (red arrow) due to the short immersion duration (2 min immersion). Subsequently, with a longer immersion duration, more suspension penetrated into the NB film (white arrows), resulting in a thicker M layer. The thickness for 5 min immersion increased to over 600 nm as shown in Fig. 2d. The increased diffusivity promoted higher hydrogen bond density between PVA, UG, ZnO and fiber molecules, leading to enhanced strong crosslinking interactions. This phenomenon is confirmed by the FTIR curve showing a shift of the O-H stretching vibration wavenumber from high to low wavenumber after the immersion (Fig. 3b).

3.3. *FTIR spectra*

The FTIR curve was utilized to monitor the structural changes of each film via shifts of peak intensity, broadening of peaks, and the appearance or disappearance of bands [51]. Fig. 3a displays the FTIR spectra from 4000 to 250 cm^{-1} for all samples. It can be seen that the main peaks for NB0 (BC) were observed at 3338, 2894, 1604, 1314, and 1054 cm^{-1}. These peaks are corresponding to stretching vibration of the O-H (hydroxyl) bond, C-H (methylene) bond, C=C bond, bending

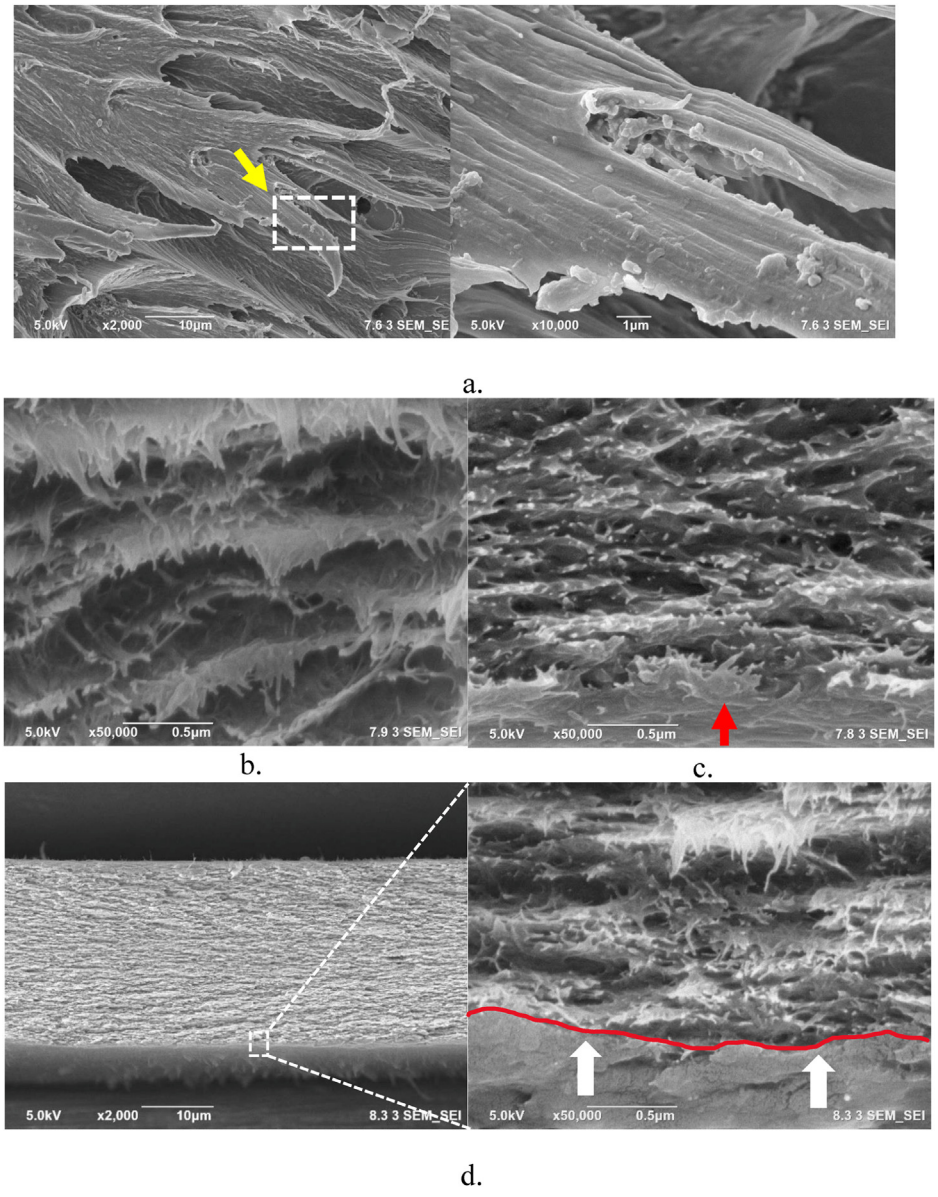

Fig. 2 – FESEM fracture surface in the cross-section of tensile samples for the BC film (a), matrix (M) (b), and BC/M film from an immersion of 2 min (c), and 5 min (d).

vibration of the C-H (methylene) bond, and stretching vibration of the C-O (ether) bond, accordingly [52,53]. Another significant peak appears in the range of 440–452 cm^{-1}. This peak represents the stretching vibration of the Zn-O bonds in the ZnO crystal lattice [54]. After immersion of the NB0 film in the PVA/UG/ZnO solution, noticeable changes were observed in the band intensity and the wavenumber of peaks in the FTIR curves. For instance, a new peak at a wavelength of 800 and 440–452 cm^{-1} emerged after immersion (NB2 and NB5), attributed to the presence of PVA and ZnO (M). Moreover, after a 5-min immersion, the wavenumber of OH stretching shifted from 3338 cm^{-1} (NB0 film) to 3243 cm^{-1} (the NB5 film) (Fig. 3b). This finding is attributed to an increase in hydrogen bond density resulting from greater contact between BC nanofiber surfaces and the matrix [55]. The higher contact ratio led to a reduction in free hydroxyl groups, as confirmed by weakening peak intensity (the increased transmittance (T) value) [56]. The NB0 film exhibited the lowest T value of OH stretching (64%), indicating the highest fraction of free hydroxyl fraction [57]. After immersion in the matrix, the OH stretching intensity weakened. For instance, the T value related to OH group for the NB0 sample is 71%, which shifted to 79% for NB2. The weakest peak intensity of these OH groups was observed on the NB5 film (T = 82%), indicating the lowest number of free OH groups. The decreased numbers of free OH groups result from the increased interfacial hydrogen bonding between the BC nanofibers and the matrix [58].

3.4. *X-ray diffraction*

Fig. 4 displays the XRD curves for NB0, NB2, NB5, and M films. The biocomposite films exhibit a similar pattern with two

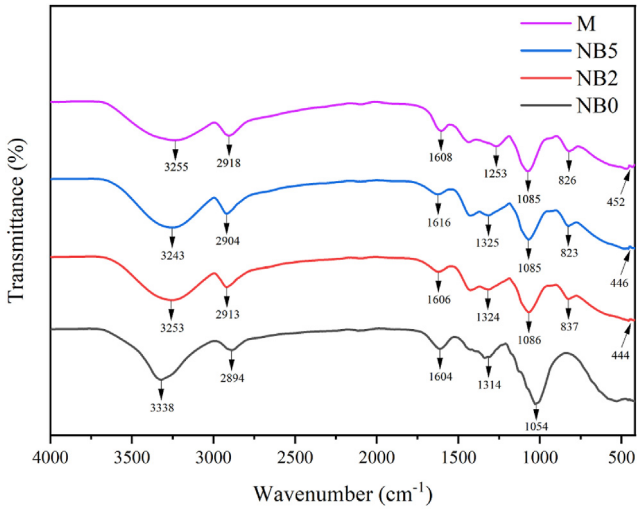

Fig. 3 – FTIR spectra of all studied films with the spectrum expanded to present changes in peaks related to specific functional groups.

distinct diffraction peaks at approximately 2θ = 14.4° and 22.7°, corresponding to the (110) and (200) lattice planes [59]. This pattern confirms the presence of the typical cellulose I structure [60]. For the NB0 film, the crystal plane position was recorded at 2θ = 22.8 initially, shifting to 2θ = 22.4 after a 5-min immersion (Table 1). The M sample crystal position was recorded at 2θ = 19.6. According to the literature, this is correspond to PVA [49,51]. The crystallinity index (CI) decreased from 89% (NB0) to 68% (NB5) indicating a disruption of the crystal structure toward amorphous networks. This reduction in crystallinity index is attributed to the presence of M sample, which exhibits a low CI (66%). Furthermore, this finding confirms that the sample with a longer immersion duration has a CI value close to that of M, indicating that the longer the immersion duration, the higher the concentration

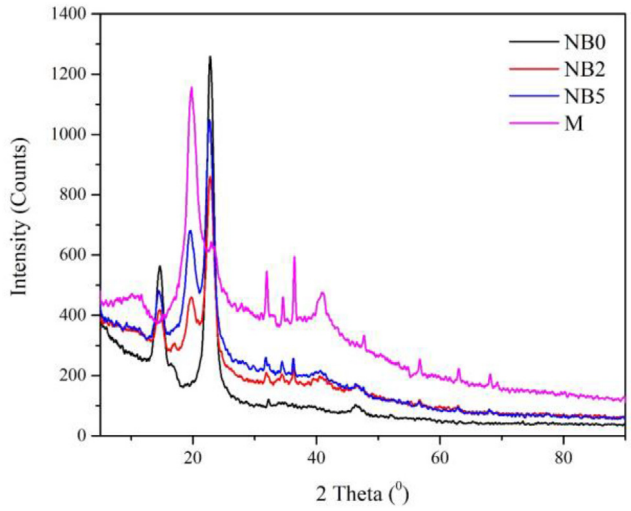

Fig. 4 – XRD patterns for NB0, NB2, NB5 and M film.

Table 1 – The crystallinity index (CI) from XRD, *d*-spacing of (200) plane from Fig. 4, T_{max}, and decomposition rate from Fig. 5.

Sample	2θ of (200) plane	CI (%) of (200) plane	*d*-spacing [Å] of (200) plane	T_{max} (°C)
NB0	22.75	88.58	3.91	317.8
NB2	22.71	70.30	3.92	322.0
NB5	22.43	67.89	3.96	325.5
M	19.58	66.17	4.53	327.1

of the PVA/UG/ZnO (M). This is consistent with the SEM results.

3.5. *Thermal properties*

Fig. 5 displays the TGA (a) and DTG (b) curves for all measured films. Initially, slight weight loss of the samples was observed due to the evaporation of absorbed water (60–150 °C) (Fig. 5a). A sudden second weight loss at 300–420 °C corresponds to cellulose and matrix decomposition. At this stage, temperatures of the maximum decomposition rate (T_{max}) for films are recorded, and their values are listed in Table 1. The matrix (M sample) exhibited the highest T_{max} at 327.1 °C. Notably, after immersion with M, biocomposite films displayed enhanced thermal resistance. Immersion of 2 and 5 min increased the T_{max} from 317.8 °C (NB0) to 322.0 °C (NB2) and 325.5 °C (NB5), respectively. This shift in temperature is attributed to increased crosslinked BC nanofiber density with the matrix and a reduction in voids within the BC film [61]. These findings were confirmed by *FESEM morphologies* (Fig. 2a and b), revealing a lower number of defects in the immersed film than the non-immersed one. Consequently, the densely packed cellulose nanofibers, resulting from strong crosslinked hydrogen bonding, lead to a higher activation energy [62]. As a result, the decomposition of the NB5 film requires much more thermal energy compared to the NB0 film. This finding aligns with previous works [63].

3.6. *Tensile properties*

Fig. 6a shows uniaxial stress-strain curves for all samples. The NB0 displays low elastic and plastic regions (Fig. 6b), confirming low toughness. This result is due to the low compactness of BC nanofiber structures, as shown in Fig. 2a. After immersion of the NB0 with PVA/UG/ZnO solution, some tensile properties of the BC/M biocomposite increased (Fig. 6c, e, and f), however, tensile modulus reduced (Fig. 6d). Immersion time of 5 min results in maximum value for tensile strength (77.2 MPa), elongation at break (12.3%), and toughness (5.8 MJ/m3). These increased by 130%, 748%, and 2409% respectively; compared to the NB0 film. A possible reason for dramatically improved tensile properties was a reduction in defects in biocomposite films. The micro- and nanosized porosities decreased and interlinked-hydrogen bonding between fibers and matrix increased. The density of the structure in the BC/M film became higher, as shown by FESEM images in Fig. 2c. These results improve the compatibility of chain structures, consequently increasing tensile properties [61].

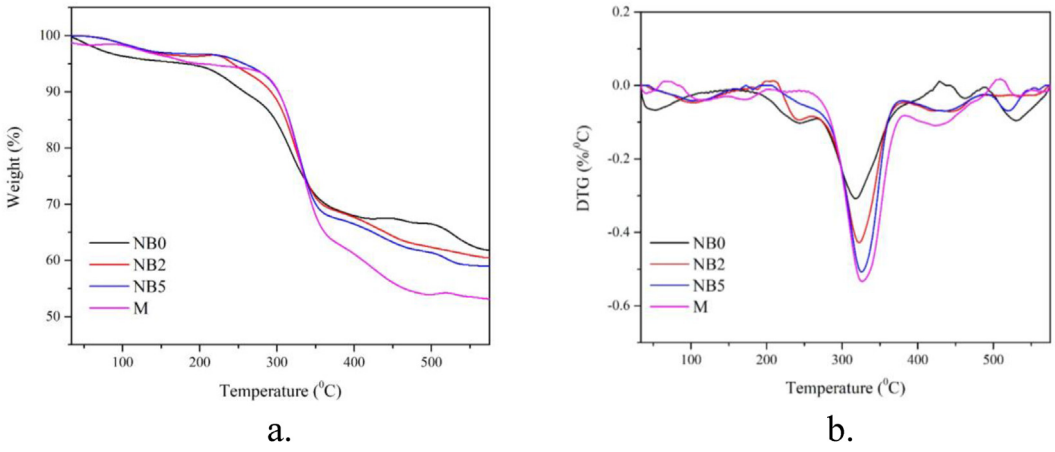

Fig. 5 – TGA (a) and DTG (b) for NB0, NB2, NB5 and M film.

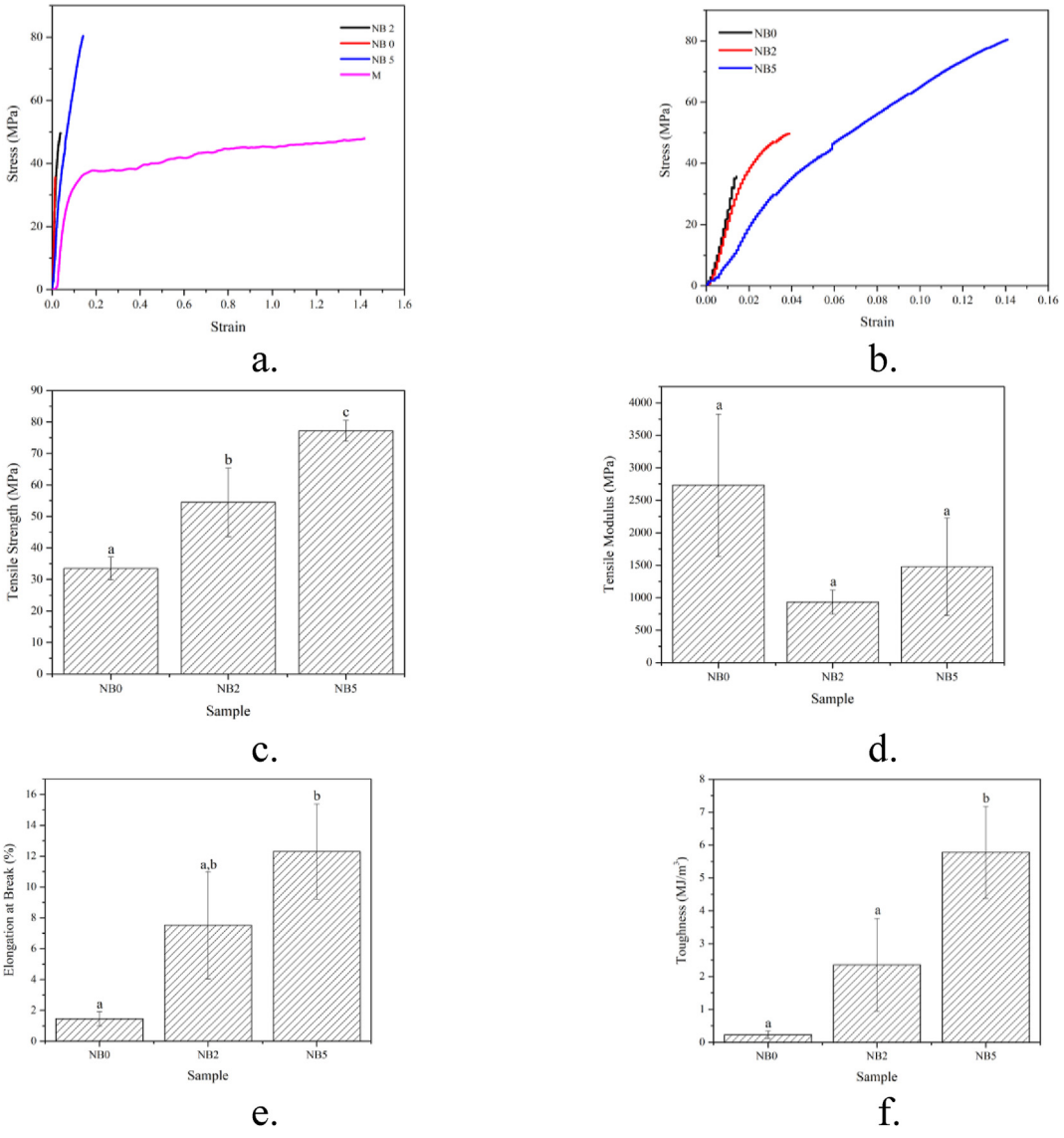

Fig. 6 – Stress-strain curve for all films (a), and without M sample (b). Average values of TS (c), TM (d), EB (e), and TN (f) for films. Different lower-case letters indicate a significant difference in mean values ($p \leq 0.05$). The same letter shows values are not significantly different.

This is also suggested by the stress-strain curve which has an extensive plastic region for NB5 (Fig. 6b) and the hydrogen-hydrogen interaction which can be implied from wave-number shifting of O-H groups for immersed films (Fig. 3). Moreover, the remarkable toughness observed in the NB5 film can likely be attributed to increased plasticization and inter-fibrillar slippage, resulting in a large strain-to-failure [48]. The extended immersion duration provides the polymer with more time to penetrate deeper into the paper fibers, fostering enhanced adhesion and bonding between PVA molecules and the BC film, consequently leading to improved tensile strength. As the duration of immersion increases, the concentration of PVA also rises. Notably, PVA exhibits superior strength compared to BC. The flexibility in PVA's molecular chains allows it to absorb more energy during deformation, leading to higher toughness and tensile strength.

4. Conclusions

We have successfully developed strong, tough, and UV light-resistant biocomposite films by immersing sonicated BC powder-based film in a PVA/UG/ZnO (M) suspension. The BC/M biocomposite film exhibited exceptional UV light absorption and had high thermal resistance. Interestingly, a 5-min immersion duration resulted in a significant increase in tensile strength, elongation at break, and toughness of the biocomposite by 130%, 748%, and 2409%, respectively, compared to the BC film. Therefore, this simple, relatively inexpensive, and environmentally friendly method holds promise for producing UV shielding food packaging and other applications requiring a visibly transparent, yet UV-resistant film.

Declaration of competing interest

The authors declare that they have no known competing financial interests or personal relationships that could have appeared to influence the work reported in this paper.

Acknowledgment

Acknowledgments are addressed to Andalas University for supporting through research funding with the project name "Skema Riset Kolaborasi Indonesia (RKI) Skema C (Host)", Number: 10/UN16.19/PT.01.03/Energi-RKI Skema C (Host)/2023.

REFERENCES

[1] Turbak A, Snyder F, Sandberg K. Microfibrillated cellulose, A new cellulose product: properties, uses, and commercial potential. J Appl Polym Sci 1983:815–27.
[2] Sharif SNM, Hashim N, Isa IM, Bakar SA, Saidin MI, Ahmad MS, et al. Polymeric nanocomposite-based herbicide of carboxymethyl cellulose coated-zinc/aluminium layered double hydroxide-quinclorac: a controlled release purpose for agrochemicals. J Polym Environ 2021;29:1817–34. https://doi.org/10.1007/s10924-020-01997-0.
[3] Rakhmania CD, Sari SR, Azhar YI, Sugita A, Tominaga M. Cellulose nanofiber platform for electrochemical sensor device: impedance measurement characterization and its application for ethanol gas sensor. Teknomekanik 2022;5:57–62. https://doi.org/10.24036/teknomekanik.v5i1.12872.
[4] Zakani B, Entezami S, Grecov D, Salem H, Sedaghat A. Effect of ultrasonication on lubrication performance of cellulose nano-crystalline (CNC) suspensions as green lubricants. Carbohydr Polym 2022;282:119084. https://doi.org/10.1016/j.carbpol.2021.119084.
[5] Abdel-karim AM, Salama AH, Hassan ML. Electrical conductivity and dielectric properties of nanofibrillated cellulose thin films from bagasse. J Phys Org Chem 2018;31:1–9. https://doi.org/10.1002/poc.3851.
[6] Lin D, Liu Z, Shen R, Chen S, Yang X. Bacterial cellulose in food industry: current research and future prospects. Int J Biol Macromol 2020;158:1007–19. https://doi.org/10.1016/j.ijbiomac.2020.04.230.
[7] Gabilondo N, Alon AE. A review of bacterial cellulose : sustainable production from agricultural waste and applications in various fields. Cellulose 2021;4:8229–53. https://doi.org/10.1007/s10570-021-04020-4.
[8] Xi J, Lou Y, Chu Y, Meng L, Wei H, Dai H, et al. High-flux bacterial cellulose ultrafiltration membrane with controllable pore structure. Colloids Surfaces A Physicochem Eng Asp 2023;656:130428. https://doi.org/10.1016/j.colsurfa.2022.130428.
[9] de Souza TC, Amorim JDP de, Silva Junior CJG da, de Medeiros ADM, Santana Costa AF de, Vinhas GM, et al. Magnetic bacterial cellulose biopolymers: production and potential applications in the electronics sector. Polymers 2023;15:1–15. https://doi.org/10.3390/polym15040853.
[10] Rahmadiawan D, Abral H, Kotodeli RA, Sugiarti E, Muslimin AN, Admi RI, et al. A novel highly conductive, transparent, and strong pure-cellulose film from TEMPO-oxidized bacterial cellulose by increasing sonication power. Polymers 2023;15:643. https://doi.org/10.3390/polym15030643.
[11] Fuadi Z, Rahmadiawan D, Kurniawan R, Mulana F, Abral H. Effect of graphene nanoplatelets on tribological properties of bacterial. Cellulose/Polyolester Oil 2022;8:1–11. https://doi.org/10.3389/fmech.2022.810847.
[12] Abral H, Kurniawan A, Rahmadiawan D, Handayani D, Sugiarti E, Muslimin AN. Highly antimicrobial and strong cellulose-based biocomposite film prepared with bacterial cellulose powders, Uncaria gambir, and ultrasonication treatment. Int J Biol Macromol 2022;208:88–96. https://doi.org/10.1016/j.ijbiomac.2022.02.154.
[13] Almuqati RR, Alamri AS, Almuqati NR. Knowledge, attitude, and practices toward sun exposure and use of sun protection among non-medical, female, university students in Saudi Arabia: a cross-sectional study. Int J Women's Dermatology 2019;5:105–9. https://doi.org/10.1016/j.ijwd.2018.11.005.
[14] Vilela C, Pinto RJB, Coelho J, Domingues MRM, Daina S, Sadocco P, et al. Bioactive chitosan/ellagic acid films with UV-light protection for active food packaging. Food Hydrocolloids 2017;73:120–8. https://doi.org/10.1016/j.foodhyd.2017.06.037.
[15] Patil AS, Waghmare RD, Pawar SP, Salunkhe ST, Kolekar GB, Sohn D, et al. Photophysical insights of highly transparent, flexible and re-emissive PVA @ WTR-CDs composite thin fi lms: a next generation food packaging material for UV blocking applications. J Photochem Photobiol Chem 2020;400:112647. https://doi.org/10.1016/j.jphotochem.2020.112647.
[16] Sadeghifar H, Venditti R, Jur J, Gorga RE, Pawlak JJ. Cellulose-lignin biodegradable and flexible UV protection film. ACS

Sustainable Chem Eng 2017;5:625–31. https://doi.org/10.1021/acssuschemeng.6b02003.
[17] Nafchi AM, Alias AK, Mahmud S, Robal M. Antimicrobial, rheological, and physicochemical properties of sago starch films filled with nanorod-rich zinc oxide. J Food Eng 2012;113:511–9.
[18] Zhao Z, Mao A, Gao W, Bai H. A facile in situ method to fabricate transparent, flexible polyvinyl alcohol/ZnO film for UV-shielding. Compos Commun 2018;10:157–62. https://doi.org/10.1016/j.coco.2018.09.009.
[19] Yang W, Ding H, Qi G, Li C, Xu P, Zheng T, et al. Highly transparent PVA/nanolignin composite films with excellent UV shielding, antibacterial and antioxidant performance. React Funct Polym 2021;162:104873. https://doi.org/10.1016/j.reactfunctpolym.2021.104873.
[20] Wang Q, Du H, Zhang F, Zhang Y, Wu M, Yu G, et al. Flexible cellulose nanopaper with high wet tensile strength, high toughness and tunable ultraviolet blocking ability fabricated from tobacco stalk: via a sustainable method. J Mater Chem A 2018;6:13021–30. https://doi.org/10.1039/c8ta01986j.
[21] Roy S, Kim HC, Kim JW, Zhai L, Zhu QY, Kim J. Incorporation of melanin nanoparticles improves UV-shielding, mechanical and antioxidant properties of cellulose nanofiber based nanocomposite films. Mater Today Commun 2020;24:100984. https://doi.org/10.1016/j.mtcomm.2020.100984.
[22] Li P, Sirviö JA, Haapala A, Khakalo A, Liimatainen H. Anti-oxidative and UV-absorbing biohybrid film of cellulose nanofibrils and tannin extract. Food Hydrocolloids 2019;92:208–17.
[23] Ji Y, Xu Q, Jin L, Fu Y. Cellulosic paper with high antioxidative and barrier properties obtained through incorporation of tannin into kraft pulp fibers. Int J Biol Macromol 2020;162:678–84. https://doi.org/10.1016/j.ijbiomac.2020.06.101.
[24] Abral H, Ikhsan M, Rahmadiawan D, Handayani D, Sandrawati N, Sugiarti E, et al. Anti-UV, antibacterial, strong, and high thermal resistant polyvinyl alcohol/Uncaria gambir extract biocomposite film. J Mater Res Technol 2022;17:2193–202. https://doi.org/10.1016/j.jmrt.2022.01.120.
[25] Rahmadiawan D, Fuadi Z, Kurniawan R, Abral H, Ilhamsyah F, Arafat A, et al. Tribological properties of aqueous carboxymethyl cellulose/uncaria gambir extract as novel anti-corrosion water-based lubricant. Tribol Ind 2022;44:584–91. https://doi.org/10.24874/TI.1357.08.22.10.
[26] Nandika D, Syamsu K, Arinana, Kusumawardhani DT, Fitriana Y. Bioactivities of catechin from gambir (uncaria gambir roxb.) against wood-decaying fungi. Bioresources 2019;14:5646–56. https://doi.org/10.15376/biores.14.3.5646-5656.
[27] Ho T-J, Tsai P-H, Hsieh C-H, Lin J-H, Lin Y-W, Wu J-R, et al. Role of herbal extracts of catechu from uncaria gambir in the treatment of chronic diabetic wounds. Pharmaceuticals 2022;16:66. https://doi.org/10.3390/ph16010066.
[28] Rahmadiawan D, Abral H, Railis RM, Iby IC, Mahardika M, Handayani D, et al. The enhanced moisture absorption and tensile strength of PVA/uncaria gambir extract by boric acid as a highly moisture-resistant, anti-UV, and strong film for food packaging applications. J Compos Sci 2022;6:337. https://doi.org/10.3390/jcs6110337.
[29] Rahmadiawan D, Ilhamsyah F, Abral H, Laghari IA, A Y. Effect of sonication to the stability properties of carboxymethyl cellulose/uncaria gambir extract water-based lubricant. Teknomekanik 2022;5:97–102. https://doi.org/10.24036/teknomekanik.v5i2.16972.
[30] Zhai Y, Wang J, Wang H, Song T, Hu W, Li S. Preparation and characterization of antioxidative and UV-protective larch bark tannin/PVA composite membranes. Molecules 2018;23:2073. https://doi.org/10.3390/molecules23082073.
[31] Chou CT, Shi SC, Chen TH, Chen CK. Nanocellulose-reinforced, multilayered poly(vinyl alcohol)-based hydrophobic composites as an alternative sealing film. Sci Prog 2023;106:1–15. https://doi.org/10.1177/00368504231157142.
[32] Bazzi M, Shabani I, Mohandesi JA. Enhanced mechanical properties and electrical conductivity of Chitosan/Polyvinyl Alcohol electrospun nanofibers by incorporation of graphene nanoplatelets. J Mech Behav Biomed Mater 2022;125:104975. https://doi.org/10.1016/j.jmbbm.2021.104975.
[33] Yihun FA, Ifuku S, Saimoto H, Yihun DA. Thermo-mechanically improved polyvinyl alcohol composite films using maleated chitin nanofibers as nano-reinforcement. Cellulose 2021;28:2965–80. https://doi.org/10.1007/s10570-021-03719-8.
[34] Gutha Y, Pathak JL, Zhang W, Zhang Y, Jiao X. Antibacterial and wound healing properties of chitosan/poly(vinyl alcohol)/zinc oxide beads (CS/PVA/ZnO). Int J Biol Macromol 2017;103:234–41. https://doi.org/10.1016/j.ijbiomac.2017.05.020.
[35] Li Z, Xu W, Wang X, Jiang W, Ma X, Wang F, et al. Fabrication of PVA/PAAm IPN hydrogel with high adhesion and enhanced mechanical properties for body sensors and antibacterial activity. Eur Polym J 2021;146:110253. https://doi.org/10.1016/j.eurpolymj.2020.110253.
[36] Sarwar MS, Niazi MBK, Jahan Z, Ahmad T, Hussain A. Preparation and characterization of PVA/nanocellulose/Ag nanocomposite films for antimicrobial food packaging. Carbohydr Polym 2018;184:453–64. https://doi.org/10.1016/j.carbpol.2017.12.068.
[37] Voronova MI, Surov OV, Guseinov SS, Barannikov VP, Zakharov AG. Thermal stability of polyvinyl alcohol/nanocrystalline cellulose composites. Carbohydr Polym 2015;130:440–7. https://doi.org/10.1016/j.carbpol.2015.05.032.
[38] Channa IA, Ashfaq J, Gilani SJ, Shah AA, Chandio AD, Jumah MN Bin. UV blocking and oxygen barrier coatings based on polyvinyl alcohol and zinc oxide nanoparticles for packaging applications. Coatings 2022;12. https://doi.org/10.3390/coatings12070897.
[39] Hezma AM, Rajeh A, Mannaa MA. An insight into the effect of zinc oxide nanoparticles on the structural, thermal, mechanical properties and antimicrobial activity of Cs/PVA composite. Colloids Surfaces A Physicochem Eng Asp 2019;581:123821. https://doi.org/10.1016/j.colsurfa.2019.123821.
[40] P K, S S V, Narayanan BN. Ball-mill assisted green one-pot synthesis of ZnO/graphene nanocomposite for selective electrochemical sensing of aquatic pollutant 4-nitrophenol. Teknomekanik 2021;4:64–71. https://doi.org/10.24036/TEKNOMEKANIK.V4I2.10872.
[41] Zhang R, Wang Y, Ma D, Ahmed S, Qin W, Liu Y. Effects of ultrasonication duration and graphene oxide and nano-zinc oxide contents on the properties of polyvinyl alcohol nanocomposites. Ultrason Sonochem 2019;59:104731. https://doi.org/10.1016/j.ultsonch.2019.104731.
[42] Fernandes I de AA, Maciel GM, Ribeiro VR, Rossetto R, Pedro AC, Haminiuk CWI. The role of bacterial cellulose loaded with plant phenolics in prevention of UV-induced skin damage. Carbohydr Polym Technol Appl 2021;2:100122. https://doi.org/10.1016/j.carpta.2021.100122.
[43] Qiu J, Li M, Ding M, Yao J. Cellulose tailored semiconductors for advanced photocatalysis. Renew Sustain Energy Rev 2022;154:111820. https://doi.org/10.1016/j.rser.2021.111820.
[44] Huang K, Wang Y. Recent applications of regenerated cellulose films and hydrogels in food packaging. Curr Opin Food Sci 2022;43:7–17.
[45] Cazón P, Velázquez G, Vázquez M. Characterization of bacterial cellulose films combined with chitosan and polyvinyl alcohol: evaluation of mechanical and barrier

properties. Carbohydr Polym 2019;216:72–85. https://doi.org/10.1016/j.carbpol.2019.03.093.
[46] ASTM Standard D1003. Standard test method for haze and luminous transmittance of transparent plastics. West Conshohocken, PA: ASTM International; 2000. https://doi.org/10.1520/D1003-00. www.astm.org. 2000:2000.
[47] ASTM D638-V. Standard test method for tensile properties of thin plastic sheeting. Am Soc Test Mater 2012.
[48] Henriksson M, Berglund LA, Isaksson P, Lindström T, Nishino T. Cellulose nanopaper structures of high toughness. Biomacromolecules 2008;9:1579–85. https://doi.org/10.1021/bm800038n.
[49] Liu D, Cui Z, Shang M, Zhong Y. A colorimetric film based on polyvinyl alcohol/sodium carboxymethyl cellulose incorporated with red cabbage anthocyanin for monitoring pork freshness. Food Packag Shelf Life 2021;28:100641. https://doi.org/10.1016/j.fpsl.2021.100641.
[50] Levi L, Mueller TJJ. Multicomponent syntheses of functional chromophores. Chem Soc Rev 2016;45:2825–46. https://doi.org/10.1039/C5CS00805K.
[51] Prajapati RK, Kumar H, Saroj AL. Formation of silver particles in [PVA:CS:PEG]-AgNO3 based biopolymer electrolyte membranes: structural and electric transport properties study. Phys B Condens Matter 2023;662:414962. https://doi.org/10.1016/j.physb.2023.414962.
[52] Halib N, Amin HCIM, Ahmad I. Physicochemical properties and characterization of nata de Coco from local food industries as a source of cellulose (sifat fizikokimia dan pencirian nata de Coco daripada industri makanan tempatan sebagai sumber selulosa). Sains Malays 2012;41:205–2011.
[53] Junaidi Z, Azlan NM. Optimization of bacterial cellulose production from pineapple waste: effect of temperature, pH and concentration. In: 5th eng conf "engineering towar chang - empower green solut; 2012. p. 1–7.
[54] Kharazmi A, Faraji N, Hussin RM, Saion E, Yunus WMM, Behzad K. Structural, optical, opto-thermal and thermal properties of ZnS-PVA nanofluids synthesized through a radiolytic approach. Beilstein J Nanotechnol 2015;6:529–36. https://doi.org/10.3762/bjnano.6.55.
[55] Abral H, Chairani MK, Rizki MD, Mahardika M, Handayani D, Sugiarti E, et al. Characterization of compressed bacterial cellulose nanopaper film after exposure to dry and humid conditions. J Mater Res Technol 2021;11:896–904. https://doi.org/10.1016/j.jmrt.2021.01.057.
[56] Abral H, Anugrah AS, Hafizulhaq F, Handayani D, Sugiarti E, Muslimin AN. Effect of nanofibers fraction on properties of the starch based biocomposite prepared in various ultrasonic powers. Int J Biol Macromol 2018;116:1214–21.
[57] Kondo T. The assignment of IR absorption bands due to free hydroxyl groups in cellulose. Cellul 1997;4:281–92. https://doi.org/10.1023/A. 4, 281±292.
[58] Abral H, Kadriadi, Mahardika M, Handayani D, Sugiarti E, Muslimin AN. Characterization of disintegrated bacterial cellulose nanofibers/PVA bionanocomposites prepared via ultrasonication. Int J Biol Macromol 2019;135:591–9.
[59] Wong SS, Kasapis S, Tan YM. Bacterial and plant cellulose modification using ultrasound irradiation. Carbohydr Polym 2009;77:280–7.
[60] Erbas Kiziltas E, Kiziltas A, Gardner DJ. Synthesis of bacterial cellulose using hot water extracted wood sugars. Carbohydr Polym 2015;124:131–8. https://doi.org/10.1016/j.carbpol.2015.01.036.
[61] Abral H, Atmajaya A, Mahardika M, Hafizulhaq F, Kadriadi, Handayani D, et al. Effect of ultrasonication duration of polyvinyl alcohol (PVA) gel on characterizations of PVA film. J Mater Res Technol 2020;9:2477–86. https://doi.org/10.1016/j.jmrt.2019.12.078.
[62] Abral H, Ariksa J, Mahardika M, Handayani D, Aminah I, Sandrawati N, et al. Transparent and antimicrobial cellulose film from ginger nanofiber. Food Hydrocolloids 2020;98:105266. https://doi.org/10.1016/j.foodhyd.2019.105266.
[63] George J, Ramana KV, Bawa AS, Siddaramaiah. Bacterial cellulose nanocrystals exhibiting high thermal stability and their polymer nanocomposites. Int J Biol Macromol 2011;48:50–7. https://doi.org/10.1016/j.ijbiomac.2010.09.013.